Photoelectric characteristics of TiO_2-based on thin-film solar elements with ruthenium (II) compounds

N. Yu. Sharibaev [a], A.Q. Ergashov [a], S.B. Fazliddinov [a], R.G. Ikramov [a], M.A. Yuldoshev [b,*], A.A. Abdulxayev [a]
[a]*Namangan State Technical University, I. Karimov Street 12, 160100, Namangan, Uzbekistan,*
[b]*Turan International University, Q. Mamarasulov street, 10D house, 160106, Namangan, Uzbekistan*

Highly sensitive dye solar cell (DSSC) characteristics in preparation and use of effective methods depending on the external influence, their electrical, photoelectric and photovoltaic characteristics have been studied. The temperature dependence with the conductivity properties of the electrolyte was studied using alternating currents of different frequencies. The results showed that the photocell assembled with TiO_2 and ruthenium photoanode had the best photogeneration ability when I_2 concentration was 0.015%. The bandgap of the sample obtained using the Taus method based on the Bouguer Lambert law is 0.3 mMol N_3 ($\alpha h\nu^{1/2}$, $cm^{-1/2}$, $eV^{1/2}$=0.99) (E_g=1.804 eV: 1.603eV). For the created thin film solar cell, the conductivity value of the sample was calculated to be σ =0.0493378 Ω^{-1} with the help of obtaining and analyzing the photoelectric characteristics of the impedance spectroscopy method.

(Received October 2, 2025; Accepted December 19, 2025)

Keywords: Semiconductor, Photoanod, Photogeneration, Conductivity, Sensitivity, Impedance analyzer

1. Introduction

Over the past ten years, numerous investigations have been carried out on various aspects of dye-sensitized solar cells (DSSCs) [1]. Among them, Shalini and co-researchers explored the characteristics of sensitive layers incorporating ruthenium complexes, metal-free organic dyes, quantum dot sensitizers, perovskite-based dyes, and both synthetic and natural organic dyes [2]. While various DSSC components have been evaluated, the review by Yang *et al*. [3] and Wu *et al*. [4] primarily emphasized the electrode section. Their analysis covered diverse counter electrode types, focusing on factors like transparency, flexibility, and materials such as metals and their alloys, carbon-based substances, conductive polymers, and metallic compounds [5]. Furthermore, they categorized photoanode modifications into three main types: coating and scattering layers, compositional changes, and inclusion of both non-metallic anions and metallic cations [6]. By examining previous literature and comparative reviews, researchers have developed efficient methodologies to evaluate the evolution of DSSCs and assess the current advancements in each component, making them applicable for DSSC integration [7]. Ruthenium (II)-based TiO_2 solar cells typically include dual transparent conductive layers, serving as substrates for dye deposition and acting as current collectors [8]. Common conductive glasses used in DSSCs include fluorine-doped tin oxide (FTO, SnO_2) and indium-doped tin oxide (ITO, In_2O_3: Sn) [9, 10]. The working electrode, or photoanode, is usually fabricated by applying a thin film of semiconductor oxides—such as TiO_2, Nb_2O_5, ZnO, SnO_2 (n-type), or NiO (p-type)—onto transparent conductive glass [11-13]. These oxides typically possess a wide band gap ranging from 3 to 3.2 eV. Sun *et al*. demonstrated that DSSCs using graphene-modified TiO_2 photoanodes achieved a power conversion efficiency (PCE) of 4.28%, representing a 59% improvement over cells without graphene [14]. Sharma *et al*. [15] also reported enhanced PCE values—7.35% and 8.15%—for co-

* Corresponding author: murod.yuldoshev1993@gmail.com
https://doi.org/10.15251/JOR.2025.216.859

sensitized solar cells employing graphene-modified TiO_2 (G-TiO_2) instead of pure TiO_2. Similarly, Calogero *et al*. [16] presented a low-cost, transparent counter electrode made from platinum nanoparticles, which delivered comparable solar conversion efficiency to conventional platinum-sputtered electrodes [17]. Li and collaborators demonstrated that transition metal nitrides such as MoN, WN, and Fe_2N possess electrocatalytic activity similar to platinum in DSSCs, with MoN exhibiting the highest performance. According to their J–V characterization, the cell using a MoN-based counter electrode achieved a fill factor (FF) of 0.66, surpassing that of a standard Pt electrode [18]. The basic law of light absorption is the Beer-Bouger-Lambert law, which states that the process of light extinction is linear in terms of intensity and amount of radiation [19]. Irradiation is kept constant provided that the physical state of the active substance. Sometimes non-linear processes also occur. Based on this law, the parallel conduction and valence band spacings were determined with the process of connecting each layer for the photoanide, relying on the Taus method, using the values obtained on the basis of this law [20].

2. Experimental samples and research methods

2.1. Preparations of ionic conductive medium and study of its conductivity values

Electrolyte mesoprous photoanode should take the uneven surface shape. In this work, a plan for the preparation of electrolytes with different concentrations of iodine was drawn up and used in the experiment. The electrolyte is catalyzed by an opaque electrode on the opposite side. The list of equipment and chemicals needed for electrolyte preparation: KI-potassium iodide, TBAI-Tetrabutylammonium iodide. PEO-Poly (ethylene oxide): stable at levels of 0.1% or higher in substance/mixture, Formula, $(C_2H_4O)nH_2O$, physical state as powder colloid, color pale yellow, PC-propylene carbonate: Chemical Formula-$C_4H_6O_3$, Molecular weight-102.09 g/mol, EC-Ethylene carbonate: Formula-$C_3H_4O_3$, Molecular weight-88.06 g/mol, DMF-Dimethylformamide: Chemical formula-C_3H_7NO, Molecular weight-73.09 g/mol, physically liquid, transparent state, Melting point: -61 °C, boiling point: -153 °C, pH 7 at 200 g/l at -20 °C, I_2-iodine: chemical formula I_2 , Melting point 113 °C, Initial boiling point 184 °C, the product is non-flammable, pH-5.4. These reagents have undergone high precision tests and are accepted by "Sigma-Aldrich". Electronic balance: AS ONE 2-8032-13 ASR224/E ASPRO Analytical Balance (220 g, 0.1 mg). In order to avoid measurement errors caused by air flow in the scale, the glass window is made with a shell.

In the process of measurement, close the door of the window and wait until a balanced mass indicator is formed. In the process of determining the mass of substances in the form of powder, metal or non-metal thin papers are used. In this case, their masses are taken separately in the tare share. When weighing liquids, the mass of the container is recorded with an accuracy of 0.001 mg and used to calculate the liquid mass. IKA C-MAG HS 7th device. hot plate and magnetic stirrer, with glass ceramic heating plate, the device has rotating magnetic field and high temperature mixing property. Technical data: Maximum capacity: 10 L, Speed range: 100–1500 rpm, Heating range: 50–500 °C. When choosing this device, attention is paid to keeping the magnetic field of the selected frequency constant at the selected temperature for a long time. Ultrasonic bath STARSONIC 18 model: ultrasonic bath for decontamination during sample processing. is an unheated ultrasonic bath for equipment cleaning and cold sterilization. It generates frequencies from 28 to 34 kHz. stainless steel (1.8 l) liquid container, with digital control and timer (entering working time by command based on electronic devices), can heat liquid from 20 °C to 70 °C. After the necessary equipment and chemical reagents were ready, separation works were carried out step by step with the help of an electronic scale. Thin materials, which do not interact with this substance, were used to extract the required amount of substances. For liquids, a container was used that does not react chemically with this liquid and does not wet each other. Six glass containers were selected for the preparation of electrolyte in six samples. These dishes are washed alternately first with plenty of plain water, then with foaming dishwashing detergent and distilled water. Glass containers that have been washed and cleaned are dried with the help of hot air. The chemicals necessary for the preparation of the electrolyte for the vessels are prepared in two main parts, and then they are prepared by adding them to a single vessel. If KI and TBAI are prepared separately, PEO, PC, EC, DMF are prepared separately. The work is completed by adding I_2 at the end of the preparation stage of all electrolytes. The solutions are kept in an electric

heater with a rotating driving magnetic field during the process of constant mixing, in which rotating magnetic fields with different temperatures and different frequencies were used for experimental purposes.

- 1- 0,05grKI+0,1PEO+0,25PC+0,25EC+0,5DMF+0,005I2(10%)
- 2-0,05grKI+0,0TBAI+0,1EO+0,25PC+0,25EC+0,5DMF+ 0,01I2(10%)
- 3-0,05KI+0,10TBAI+0,1PEO+0,25PC+0,25EC+0,5DMF+0,015I2(10%)
- 4-0,05KI+0,15TBAI+0,1gr PEO+0,25PC+0,25EC+0,5DMF+0,02I2(10%)
- 5-0,05KI+0,20TBAI+0,1PEO+0,25PC+0,25EC+0,5DMF+0,025I2(10%)
- 6-0,05TBAI+0,1PEO+0,25PC+0,25EC+0,5DMF+0,005I2(10%)

Electrolyte samples 1, 3, 5 were processed in an ultrasonic device for a duration of 3, 5, 7 minutes and a temperature of 20 °C, 50 °C, and 70 °C, respectively. The theoretical basis for the choice of this ignition is to cause small-amplitude vibrations in the liquid to induce catalyst function by transferring them to the sample.

After the preparation of the samples, studies of their degradation were carried out. HIOKI IM 3570 IMPEDANCE ANALYZER and BUCHI Glass Oven B-585 devices were used for this. At the beginning of the work, six samples were placed in two-electrode small-sized vessel-shaped devices. This is due to the fact that the specified surface is known during the study of permeability, which does not cause difficulties in the calculation process. A small galvanic cell is separated from each other by dielectrics, so that the liquid electrolyte heats up when it conducts an electric current and at the same time evaporates, so that it does not open or weak contact transients occur. a secondary shell with grooved grooves for mechanical fastening to the device and a part that provides contact with the data transmission line to the device is mounted on the device. The above-mentioned operations were performed more than 6–10 times for each of the six samples at room temperature and above 90 °C, in order to reduce the relative and absolute errors, it is possible to obtain results from multiple times for each sample at different temperatures. It is the main factor for the issue of interest-bearing shares.

The value of the frequencies that should be given to the IM 3570 IMPEDANCE ANALYZER-device is entered on the basis of special software. The fact that these frequencies are given to all samples at the same time makes it easier to analyze the results based on a graph [21]. Below is the Nyquist method analysis of impenads obtained on the basis of 6 electrolyte samples.

2.2. In order to obtain the photoelectric characteristics of the prepared TiO_2-based thin film efficient photovoltaic cells, the following works were carried out

Most of the DSSC-based work has been evaluated in the standard AM 1.5 case. In fact, different light sources are used in different types of laboratories, and the characteristics of the light condition, spectrum and intensity of the closed atmosphere are different. In order to complete the work according to the goal, the following two main stages are carefully considered. A) The same first sample is first analyzed by I–V curve and then by Impedance spectroscopy. B) In the alternative of this first sample, spectroscopic analysis is performed first, then I–V curve observation is performed and the results are taken for analysis. In the application of this method, all aspects should be approximated to homogeneity, including photoanodes, electrolytes, contour electrodes and dyes should be obtained on the basis of the same samples. During the implementation of this work in two stages, the processes created as a result of the initial measurement observation work are divided without any doubt that the next measurement may have an impact on the observation work. Each of these two-stage works was performed in the following sequence of actions. 1. The Nova device is started and calibration is carried out on objects with known sizes for measurement work, and the level of accuracy is determined. 2. When the device is ready for operation, the photoanodes are removed from the storage box and cleaned with ethanol. This is achieved by pouring ethanol over the photoanode and no other mechanical effects are used. 3. A thin layer of the electrolyte prepared as a sample of the main electrolyte is applied to the surface of the electrode. 4. A contour electrode is attached to the semi-finished sample. 5. The photoanode and circuit electrode are fixed with two sides that do not participate in the loss using mechanical clamps to keep the electrode tightly glued to each other. 6. The sample

is placed under a light source that provides illumination equal to sunlight, with the surface facing the source (usually vertically upwards). 7. In the process of measurement, it is necessary to calculate the current density for a unit surface; therefore, the work of covering the surfaces, which set the working surface of the photocell at a certain value, is performed. There are different methods of using metal foils, and the surface of the slot left is leveled with the working surface. 8. The working frequencies necessary for impedance spectroscopy are determined for the device and the measurement control results are obtained. In step 8, the acquisition of I–V curve or impedance spectroscopy results is selected according to a previously defined plan.

2.3. Determining the width of the object's forbidden zone based on the laws of light absorption

Radiant active substance. The intensity change along ds path obeys the law of proportionality.

$$dI_\lambda = -\beta_{e,\lambda} I_\lambda d_s \quad (1)$$

Where, β (e, λ) is the volumetric extinction coefficient. The source intensity per unit length is the coefficient of the I_λ function. The sum of the absorption coefficient and scattering coefficients for the same environment can be understood as equal to the loss coefficient for the source. The extinction coefficient (as well as the absorption and scattering coefficients) can be expressed in different forms according to the determination of the amount of substances (concentrations, mass concentrations, etc.) in the direction of light propagation. The unity of coefficients can be understood as follows. Mass coefficient-unit surface area per unit mass (cm^2g^{-1}), (m^2kg^{-1}), etc [22]. If r is the density (mass concentration) of certain types of particles (or molecules), then

$$\beta_{e,\lambda} = \rho k_{e.\lambda}, \ \ \beta_{s,\lambda} = \rho k_{s.\lambda}\ , \ \beta_{a,\lambda} = \rho k_{a.\lambda} \quad (2)$$

here, k_e, k_s, and k_a, are the total absorption, scattering, and absorption coefficients, respectively. Using the total absorption coefficient, we write the Bouguer-Lambert law for total absorption as follows.

$$dI_\lambda = -\rho k_{e,\lambda} I_\lambda ds\ , \ \ dI_\lambda = \rho k_{e,\lambda} I_\lambda ds \quad (3)$$

The extinction cross section of a particle (or molecule) in the direction of light propagation is a quantity that determines the attenuation of electromagnetic radiation by a particle (or molecule). If N is the particle (or molecule) number concentration of a certain type of particle (or molecule) of the same size, then

$$\beta_{e,\lambda} = \sigma_{e,\lambda} N, \ \ \beta_{s,\lambda} = \sigma_{s,\lambda} N, \ \beta_{a,\lambda} = \sigma_{a,\lambda} N \quad (4)$$

here, $\sigma_{e,\lambda}, \sigma_{s,\lambda}, \sigma_{a,\lambda}$ represent extinction scattering and absorption cross sections, respectively. The environment between points S1 and S2 is defined as follows

$$\tau_\lambda(s_2; s_1) = \int_{s_1}^{s_2} \beta_{e,\lambda}(s) ds \quad (5)$$

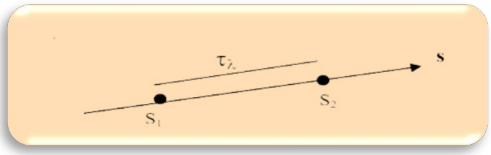

Fig. 1. Study of the ratio of light absorption to optical illusion.

If the concepts of optical depth, optical thickness, and optical path have the same meaning, if we aim to search for the general law of light absorption for space the dependence of $\beta_{e,\lambda}(s)$ on s does not depend on the direction (it is called the same optical path), thus the optical length for an electromagnetic wave can be expressed in several ways

$$\tau_\lambda(s_2; s_1) = \int_{s_1}^{s_2} \beta_{e,\lambda} ds = \int_{s_1}^{s_2} \rho k_{e,\lambda} ds = \int_{s_1}^{s_2} N \sigma_{e,\lambda} ds \quad (6)$$

If there are several optically active particles in each direction in a certain volume $\beta_{e,\lambda}$ i etc., then the optical length can be expressed as:

$$\tau_\lambda = \sum_i \int_{s_1}^{s_2} \beta_{e\lambda}^i ds = \sum_i \int_{s_1}^{s_2} \rho_i k_{e\lambda}^i ds = \sum_i \int_{s_1}^{s_2} N_i \sigma_{e\lambda}^i ds \quad (7)$$

The expressions studied above are for the application of light with a certain intensity, which spreads in a certain direction. The complete total intensity distribution at the desired angle and wavelength (or frequency) can be obtained by repeating the elementary solution for all incident rays and all wavelengths (or frequencies) [23].

Since the studied object consists of a collection of several thin layers, it is appropriate to study the physical and chemical processes along with their properties in the parts of the layers that diffuse into each other. The study of electrical conductivity, photogeneration, saturation current and other quantities in photovoltaic cells requires devices that work with high precision and observe in nanoscale units. The bandgap width of semiconductor materials determines many of the capabilities of a device made of the material. The width of the forbidden zone of the device can be learned from its Volt-Ampere description and its dependence on various external influences [24, 25].

It is possible to determine the light absorption coefficient of the medium by studying the intensity of the light passing through the medium in the initial part and after the medium in devices capable of measuring the intensity of light with high accuracy [26, 27]. This opens up the following possibilities through Bouguer-Lambert-Beer laws.

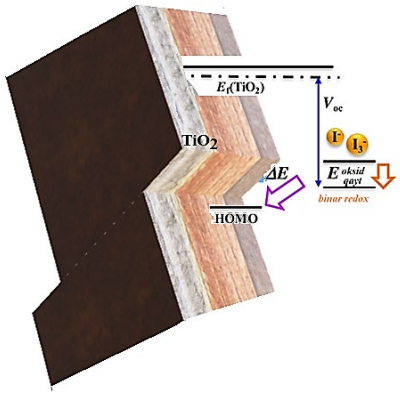

Fig. 2. Schematic explanation of photogeneration and internal conductance in DSSC-type solar photovoltaic cells.

Considering the intensity of the electromagnetic wave that passed (I) and the intensity of the electromagnetic wave that did not pass through the first studied object (I_0), according to the laws of Bouguer-Lambert

$$I = I_o e^{-\alpha d} \quad (8)$$

here, is the absorption coefficient of the α-spectrum, d-the width of the sample along the electromagnetic wave. Deriving the absorption coefficient of the α-spectrum from the Bouguer-Lambert equation:

$$\frac{I}{I_o} = e^{-\alpha d}, \frac{I_o}{I} = e^{\alpha d},\ lge^{\alpha d},\ \alpha d\ ge = lg\frac{I_o}{I} \quad (9)$$

If we know the optical density A of the medium and the intensity of the incoming and outgoing rays I and I_0, respectively, the ratio between them is expressed as follows.

$$A = \lg\frac{I_0}{I} \quad (10)$$

A can be calculated instead of the resulting value of the combined optical density for several layers.

$$\lg e \approx 0.43;\quad \alpha d \lg e = A;\quad \alpha = \frac{1}{d}\frac{A}{\lg e}, \quad (11)$$

$\frac{1}{\lg e}$=const≈ 2.32 since it is invariant, expression (4) $\alpha = \frac{2.32}{d}A$ gives the working expression [1/sm], [sm^{-1}].

Using the above expressions, using the Taus method, we use the equation that connects the absorption spectrum of electromagnetic waves and the width of the forbidden zone.

$$(\alpha h\nu)^n = k(h\nu - E_g) \quad (12)$$

here, α is the absorption coefficient, k is the proportionality coefficient, hn is the photon energy, and n is the zone index of the semiconductor material. If n=2, it is a straight-band semiconductor, and if n=1/2, it is a non-straight-band semiconductor. E_g is the bandgap width of a semiconductor sample.

Photoconductivity occurs only as a result of light absorption. In this case, the relationships between photon energy, frequency and wavelength are as follows. E=hν=hc/λ where h is Planck's constant. Photoconductivity is observed in a special semiconductor E>E_g. Photoconductivity is observed in compound semiconductors in cases where E>E_d, E>E_a.

For a special semiconductor $\lambda = \frac{hc}{E_g}$, (13)

For the donor and acceptor mixture, l=hc/E_a, =hc/E_d. (22) if the thermal excitation of electrons and holes is organized in mixed semiconductor materials and taking into account this phenomenon, the expression of relative conductivity is written as follows.

$$\sigma_0 = e(n_0\mu_n + p\mu_p) \quad (14)$$

here, n_0, and p_0 are the concentrations of electrons and holes. Since the effect of light is not observed in the expression, σ_0 is called relative conductivity for the dark state. If free electrons are generated under the influence of light, it is understood as optical generation. Conductivity created at the expense of generation

$$\sigma = e(n\mu_n + p\mu_p) \quad (15)$$

In this case, n=n_0+Δn, p=p_0+Δp is the concentration of free electrons additionally formed due to photogeneration in the illuminated semiconductor material. Then, in order to determine how the photoconductivity changes under the influence of light, we make the difference between the relative conductivities calculated for the illuminated and dark conditions.

$$\Delta\sigma = \sigma - \sigma_0 = e(\Delta n\mu_n + \Delta p\mu_p) \quad (16)$$

Full conductivity depends on the concentration of thermally generated electrons in the dark and photogenerated electrons when illuminated. $\sigma = \sigma_t + \sigma_f$ Some time after the photoresist is illuminated, stable conductivity $\Delta\sigma_{turg}$ and stable concentration of electrons Δn_{turg} and holes Δp_{turg} are determined. At this time, the amount of recombining particles also increases from zero to a stable value [28]. The time until recombination of each free charge particle is called its lifetime. Average residence time is determined by t.

$$\frac{d(\Delta n)}{dt} = G - \frac{\Delta n}{\tau} \quad (17)$$

G-rate of electron and hole generation per unit volume. For a stationary photoconductor, $\frac{d(\Delta n)}{t} = 0$From the above expressions, the expression $\Delta n_{st} = G\tau$ is formed for the concentration of stationary electrons. In a special semiconductor, the concentration of holes is $\Delta p_{st} = \Delta G\tau$. Then photoconductivity

$$\Delta\sigma_{st} = e\Delta n_{st}(\mu_n + \mu_p) = Ge\tau(\mu_n + \mu_p) \quad (18)$$

The resulting expression serves as a function expressing the generation dependence of photoconductivity for semiconductors [29]. According to Bouguer's law, absorption of light in a plate of thickness

$$XN(x) = N_0 \exp(\alpha x) \quad (19)$$

here, is the α-absorption coefficient (depending on the nature of the substance and the wavelength).

$$\Delta N = N_0 - N_0 \exp(-\alpha\Delta x) = N_0(1 - \exp(-\alpha\Delta x)). \quad (20)$$

here, ΔN is the pair of electrons and holes formed as a result of photon absorption.

$$\Delta N_{juft} = \beta\Delta N = \beta N_0\alpha\Delta x \quad (21)$$

The coefficient β is called the quantum efficiency of the internal photoeffect. It shows how much of the photons absorbed in the semiconductor formed a pair of current carriers. Usually $\beta < 1$, because there are processes of electron formation even without the formation of electrons and holes [30]. For the formation of ΔN_{juft} of electron and hole pairs in unit plate thickness, their generation rates are calculated for an object with a depth of Δx.

$$G = \frac{\Delta N}{\Delta x} = \beta N_0 \alpha \tag{22}$$

The relative conductivity in the stationary state is as follows.

$$\Delta\sigma_{st} = e\beta\alpha\tau(\mu_n + \mu_p)N_0 \tag{23}$$

ν- the relationship between radiation frequency and N_0 photon flow density is derived as follows. $N_0 = \frac{P}{h\nu}$

$$\Delta\sigma_{st} = e\beta\alpha\tau(\mu_n + \mu_p)\frac{P}{h\nu} \tag{24}$$

All expression values studied above are not considered correct in relation to the real situation, because a simplified model of processes in semiconductors was considered in their creation. The actual dependence of the photocurrent on the light P may differ from the values of the linear function [31]. Usually, the dependence of the value of the photocurrent generated in the photoresistor on the wavelength of the incident light is studied [32, 33].

$$I_f = f(\lambda)_{E=const}$$

$\frac{hc}{\lambda_0} = \Delta E$ when using the expression, it is possible to determine the width of the forbidden zone by studying ΔE.

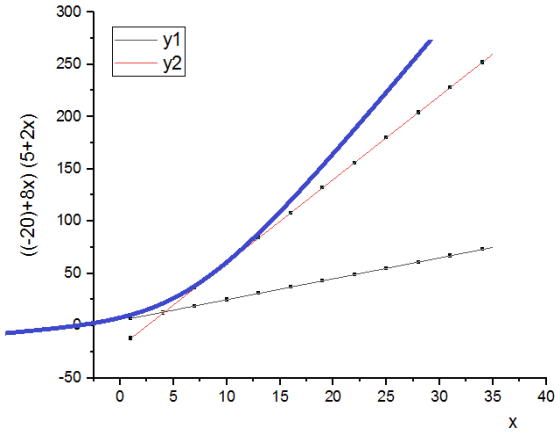

Fig. 3. Based on the Taus method, the method of studying the forbidden zone width of a sample using a graph.

Based on the formulas studied above, the width of the forbidden zone for different layers of the photoanode is determined using the Taus method [34]. For this purpose, two attempts that did not cross the curve area of the graph are drawn. After determining the coordinates of two points lying in these tests, after several mathematical steps, the coordinates of the point of intersection of these tests were obtained. The projection of this intersection point coordinate on the X-axis represents the width of the forbidden zone (E_g) for the sample in question. The calculation process can be carried out in two ways. (16) is a geometric method based on trigonometric laws and requires long calculations. 2) a method of mathematical analysis based on finding the point of intersection of functions. The coordinates of the two attempts transferred to the graph are determined accordingly. (X_1:Y_1), (X_2:Y_2), (X_3:Y_3), (X_4:Y_4) The projection of the cross section between the points obtained in each trial on the X and Y axes is found.

$$\Delta x_1 = x_2 - x_1 \quad \Delta y_1 = y_2 - y_1$$
$$\Delta x_2 = x_4 - x_3 \quad \Delta y_2 = y_4 - y_3$$
$$\text{thus} \quad \text{tg}\,\alpha_1 = \frac{\Delta y_1}{\Delta x_1} \quad \alpha = arctg\frac{\Delta y_1}{\Delta x_1} = \frac{y_2 - y_1}{x_2 - x_1} \tag{25}$$

similarly this $\text{tg}\beta_1 = \frac{\Delta x_2}{\Delta y_2}$ $\beta_1 = arctg\frac{\Delta x_2}{\Delta y_2} = \frac{x_4 - x_3}{y_4 - y_3}$ (26)

In this case, the section connecting the starting and ending points given to attempts

$$a = \sqrt{(x_4 - x_1)^2 + (y_4 - y_1)^2} \quad (27)$$

$$cos\alpha = \frac{(x_4 - x_1)}{a} = \frac{(x_4 - x_1)}{\sqrt{(x_4 - x_1)^2 + (y_4 - y_1)^2}} \rightarrow$$

$$\alpha = arccos\frac{(x_4 - x_1)}{a} \quad (28)$$

$$sin\alpha = \frac{y_4 - y_1}{a} = \frac{y_4 - y_1}{\sqrt{(x_4 - x_1)^2 + (y_4 - y_1)^2}} \rightarrow$$

$$\alpha = arcsin\frac{(y_4 - y_1)}{a} \quad (29)$$

In this practice, the opposite sides can be used interchangeably with the sine and cosine values.

Thus $\alpha - \alpha_1 = \alpha_2$ gives $\beta - \beta_1 = \beta_2$

Using the angle values obtained from the expression (41-42), it is divided into the expression g=180-(b_2+a_2). It was possible to find two unknown sides of a triangle from the ratio of the angles and their opposite sides.

$$\begin{cases} ax = \gamma \\ bx = \beta_2 \\ cx = \alpha_2 \end{cases} x = \frac{\gamma}{a}, b = \frac{b_2}{x} = \frac{b_2 * a}{\gamma}, c = \frac{\alpha_2}{x} = \frac{\alpha_2 * a}{\gamma} \quad (30)$$

After determining the sides ABC of the triangle from the expression (43), the value of the coordinate of point A on the X axis is determined.

For example: $cos\alpha_1 = \frac{\Delta x_1^1}{b} \rightarrow \Delta x_1^1 = bcos\alpha_1$ $x = x_1 + \Delta x_1^1$ projection of the intersecting point using this value. The coordinate values of points in the test, which are necessary for performing these actions, are entered using maple, matcad, origin, excel programs.

$$x = x_1 + bcos\alpha_1 = x_1 + b\sqrt{\frac{1}{tg^2\alpha_1 - 1}} = x_1 + (\frac{b_2}{\gamma})a\sqrt{\frac{1}{tg^2\alpha_1 - 1}} \rightarrow$$

$$x_1 + \left(\frac{b - b_1}{\gamma}\right)a\sqrt{\frac{1}{tg^2\alpha_1 - 1}} = \rightarrow$$

$$x_1 + \frac{\left(\arcsin\left(\frac{x_4 - x_1}{a}\right) - arctg\left(\frac{x_4 - x_3}{y_4 - y_3}\right)\right)a}{\gamma} \cdot \sqrt{\frac{1}{tg^2\alpha_1 - 1}} \quad (31)$$

The intersection points are found by finding the coefficients and initial values of the two functions lying on the coordinates of the four points obtained in the second method and equating them. The coordinates of the two attempts transferred to the graph are determined accordingly. (X_1:Y_1), (X_2:Y_2), (X_3:Y_3), (X_4:Y_4

$$\begin{cases} y_1 = k_1x_1 + b_1 \\ y_2 = k_1x_2 + b_1 \end{cases}, \begin{cases} y_3 = k_2x_3 + b_2 \\ y_4 = k_2x_4 + b_2 \end{cases} \quad (32)$$

$$y_2 = k_1x_2 + y_1 - k_1x_1 = k(x_2 - x_1) + y_1 \quad (33)$$

$$k_1 = \frac{y_2 - y_1}{x_2 - x_1}, \quad b_1 = y_1 - \frac{y_2 - y_1}{x_2 - x_1}x_1, \quad (34)$$

in the same way, the coefficients of the second function are found.

$$k_2 = \frac{y_4 - y_3}{x_4 - x_3}, \quad b_2 = y_3 - \frac{y_4 - y_3}{x_3 - x_3}x_3 \quad (35)$$

$$\text{thus } \frac{y_2 - y_1}{x_2 - x_1}x + y_1 - \frac{y_2 - y_1}{x_2 - x_1}x_1 = \frac{y_4 - y_3}{x_4 - x_3}x + y_3 - \frac{y_4 - y_3}{x_3 - x_3}x_3 \quad (36)$$

When equation (49) is solved, the intended goal is achieved.

3. Results and discussion

The following advantages can be listed in the device "Shimadzu 1900i", which meets the international requirements and norms, as today's experience in photo electronics facilitates the observation process.

1. It automatically selects the light of the desired λ wavelength.
2. Independently activates the selected lamps with the required power.
3. It can keep the illumination at a uniform value.
4. Automatically ensures the sequence of steps.
5. Draws a description of the results independently on the computer interface.
6. Digitally exports description coordinates to a computer in various formats.

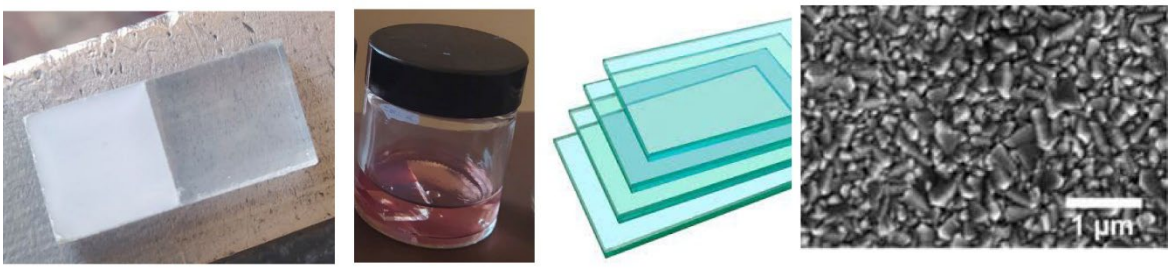

a) *b)* *c)* *d)*

Fig. 4. a) photoanode of the sample coated with TiO_2 layer. b) the condition of the anode deposited in a paint solution containing ruthenium(II). c) FTO glass parts. d) view of the photoanode on a scale of 1 micrometer.

Given the established relationship between current density and electrical conductivity, a method was investigated to evaluate conductivity under specific experimental conditions.

In different metals:

$$\rho = \rho_0(1+\alpha t)\ (17)\,, \quad \delta = \frac{1}{\rho} = \frac{1}{\rho_0(1+\alpha t)} \tag{37}$$

for Ions:

$$u_i = \left(\frac{v_0 r^2 z_i e}{kT}\right) e^{\frac{-u_i}{kT}} = \left(\frac{v_0 r^2 q}{kT}\right) e^{\frac{-u_i}{kT}} \tag{38}$$

$$\delta = C \cdot q \cdot u \quad \delta = \left(\frac{C v_0 r^2 q^2}{kT}\right) e^{\frac{-u_i}{kT}} \tag{39}$$

An oscilloscope with two channels is used to observe the form of the generated current.

In alternating current:

$$\operatorname{tg}\varphi = \frac{\omega L - \frac{1}{\omega C}}{R}\ ;\ I = I_0 \sin(\omega t), \tag{40}$$

$$U = U_0\ \sin(\omega t + \varphi) = U_0\ (\sin(\omega t)\cos(\varphi) + \sin(\varphi)\cos(\omega t)) = U_0 \tag{41}$$

$$\text{if}\ \ \frac{U_0}{I_0} = Z_0\ \ \text{bo'lsa}\ \ Z = Z_0\cos(\varphi) + Z_0\sin(\varphi)\, ctg(\omega t), \tag{42}$$

The resulting expression above can be reduced to the case of conductance in complex form, and this form is called admittance.

$$Y = \frac{1}{Z} \tag{43}$$

Using the function of the dependence of the complex resistance on the alternating current frequency (given in formula 26), it is possible to obtain the following graphs.

$$\text{If}\ \ z = x + jy \tag{44}$$

if we express conductivity through a complex expression, through Eyler's expression

$$e^{j\alpha} = cos\alpha + jsin\alpha \tag{45}$$

thus it would be.

$$\text{here,}\ \ x = \rho cos\alpha, \qquad y = \rho sin\alpha, \quad \rho = \sqrt{x^2 + y^2}, \quad tg\alpha = \frac{y}{x}, \tag{46}$$

and the trigonometric expression of impedance

$$z = \rho cos\alpha + j\rho sin\alpha \tag{47}$$

appears [35]. If we observe that the vector A rotates several times in the complex axis, its projection on the X and U axes can be understood and written as follows.

$$A_x = A_0\ \cos(\omega t + \varphi_0),\ \ A_y = jA_0\ \sin(\omega t + \varphi_0), \tag{48}$$

$\omega -$ frequency, $\varphi_0 -$ initial phase.

$$z = x + jy = A_0 \cos(\omega t + \varphi_0) + jA_0 \sin(\omega t + \varphi_0), \quad (49)$$

$$\text{or } z = A_0 e^{j\alpha} = A_0 e^{j(\omega t + \varphi_0)} = A_0 e^{j\varphi_0} e^{j\omega t} \quad (50)$$

In the course of this experiment, it is possible to study the effect of additional external influences on the conductivity of deformation, temperature, high-frequency fields, and it was possible to obtain the results with high accuracy. Using an electron timer and a high-precision sensitive oscillograph with a memory and an impedance meter, conducting research on conductivity, the following results were achieved.

3.1. The properties of conductivity in the electrolyte were based on the method of impedance spectroscopy

The analysis of impedance data is often a very difficult task, because the flow of charge current through a large number of boundaries is simply assumed to be in parallel with the resistance, the capacitive effect caused by the accumulation of charge in the double-layer region, apart from the resistive elements, is geometrically charge collection processes at the boundary must also be taken into account. The value of the frequencies that should be given to the IM 3570 IMPEDANCE ANALYZER-device is entered on the basis of special software. The fact that these frequencies are assigned to all samples at the same time makes it easier to analyze the results based on a graph [36]. Below, the most positive value of impenads obtained on the basis of 6 electrolyte samples was selected and graphed based on the Nyquist method.

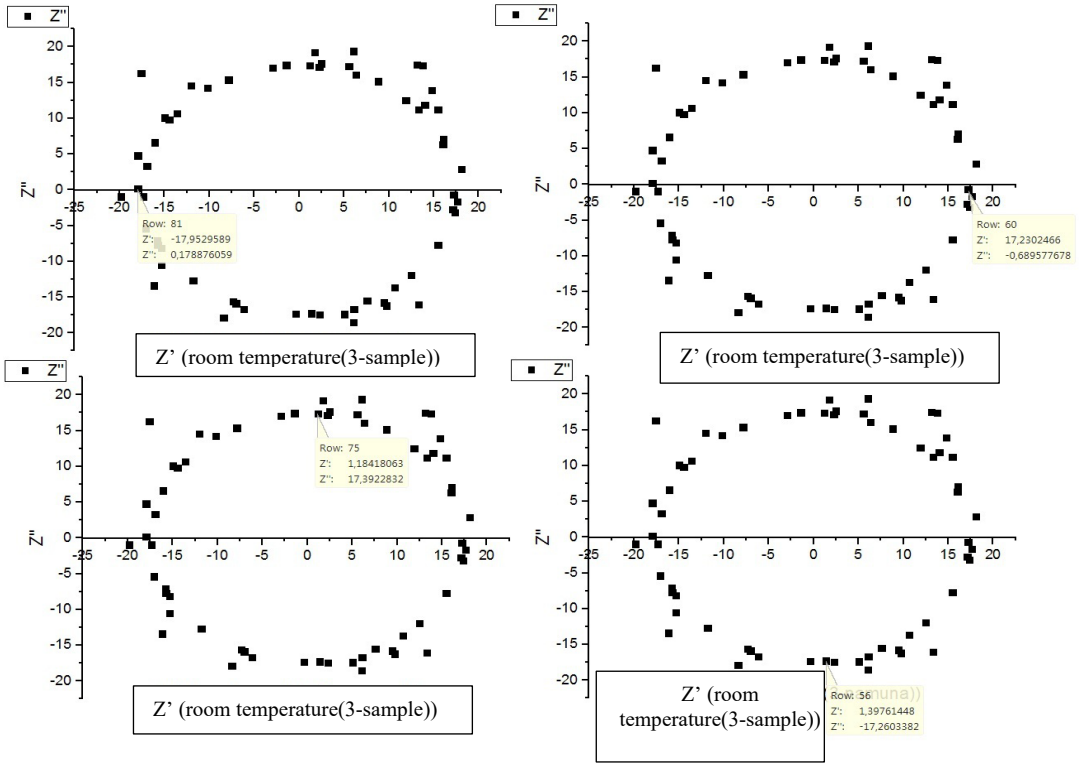

Fig. 5. Nyquist plot of electrolyte conductivity at room temperature.

3.2. Photoelectric characteristics of semiconductor and electrolyte-based solar cells

In the process of obtaining the I–V curve of the samples, it is necessary to carry out measurement and observation works for different values of the illuminance, which is mainly calculated from the external influence. In this case, constant current is used for I–V curve. In the previous chapters, values of conductivity for alternating current were studied using impedance spectroscopy method for electrolyte. It is possible to evaluate the size of the photocell by studying the effect of different values of illumination on the values of transmittance in the alternating current for the finished photocell.

For the F-0.1-0.4 mM n3 sample, I–V curve was performed 7–9 times. When obtaining the average value of the obtained result for analysis, it was possible to reduce the positive and negative shifts of the result and get the working value.

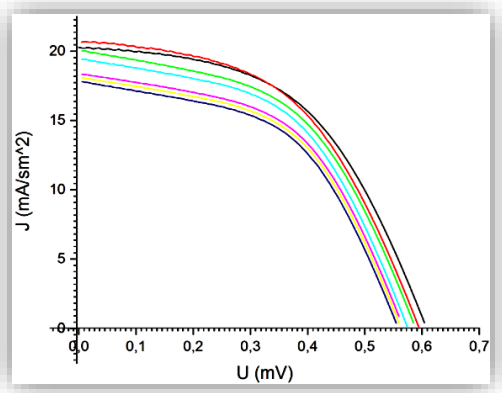

F 0.1 mMolN3

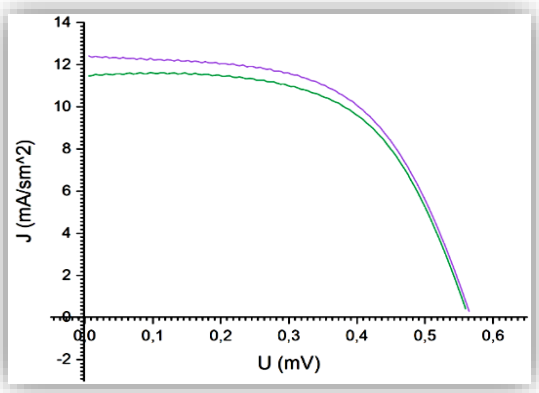

F 0.2 mMolN3

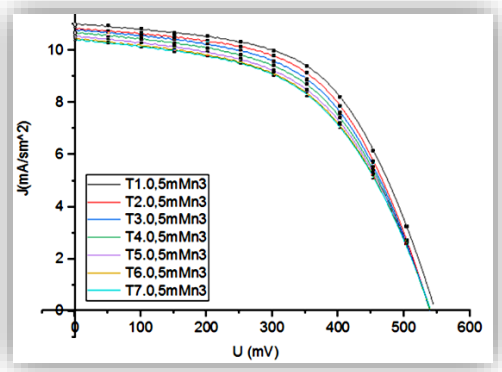

F 0.5 mMolN3

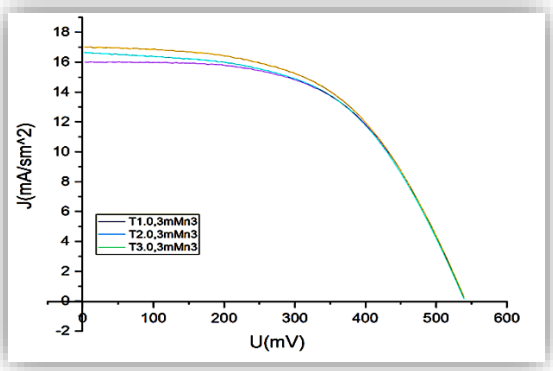

F 0.3 mMolN3

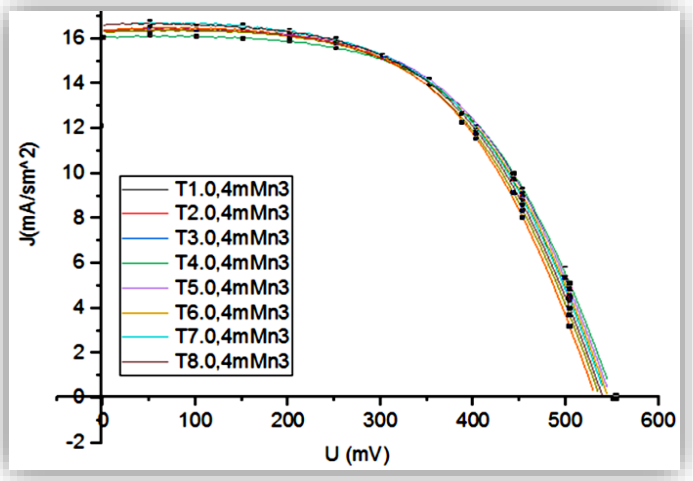

F 0.4 mMolN3

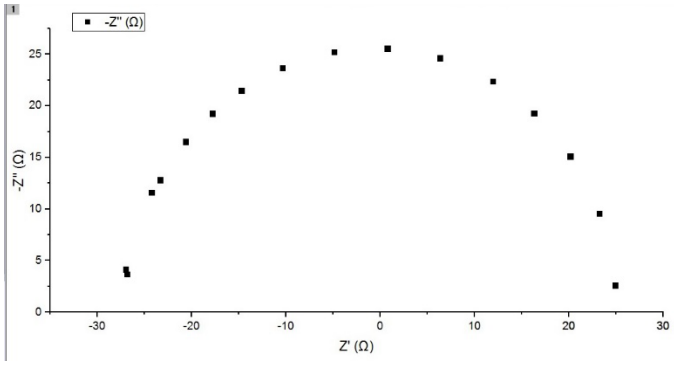

Fig. 6. For F 0.1 mMn3, a description of the monitoring of the current strength and density and an impedance analysis of the conductivity value were obtained.

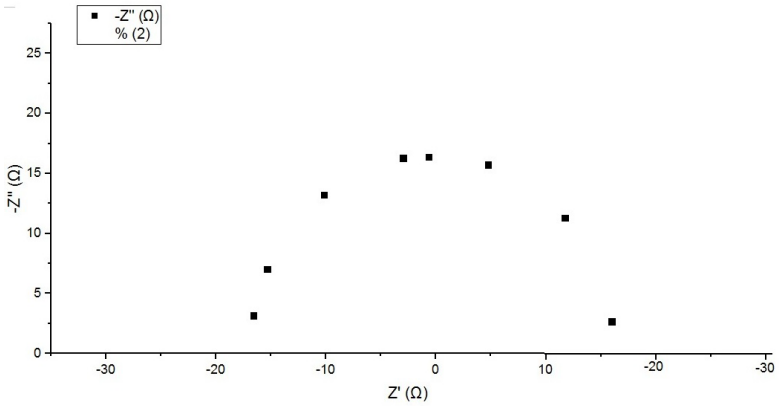

Fig. 7. For F 0.2 mMn3, a description of the observation of the current strength and density and an impedance analysis of the conductivity value were obtained.

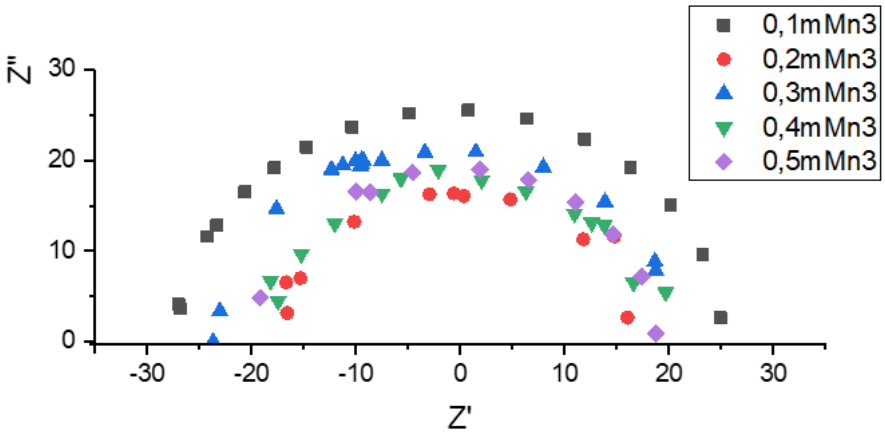

Fig. 8. (0.1:0.5- mMn3)-conductance impedance analysis for five samples summarized.

3.3. Using the Taus method, the forbidden zone width of the layers in the semiconductor photoanode was studied

Based on expressions (31) and (36) using the difference in the values of the absorbed light from the difference in intensities of the transmitted and non-transmitted light, passing a light wave

at the desired wavelength from the sample according to the previously studied Bouguer Lambert law the width of the forbidden zone is determined.

1. For the purpose of the experiment, the glass sample needed for the DSSC photocell was selected and measurements were made. In this case, optically transparent glass mainly made of silicon was used for experimental purposes. However, it is possible to use elastic and optically transparent organic glass and thin-layer films.

2. An electrode with preserved transparency is prepared by special thermal treatment of the glass window and briquetting of fluorine or indium in the case of spray. This electrode is mainly used as a photoanode.

3. Various technological methods were used to cover the prepared photoanode with TiO_2 in the form of a thin layer. These methods caused the conductivity of the DSSC part to vary, in turn, the useful work coefficient. For example, increasing the mesoprosity of TiO_2 led to an increase in the number of simultaneously absorbed photons, which led to an increase in the efficiency of photogeneration.

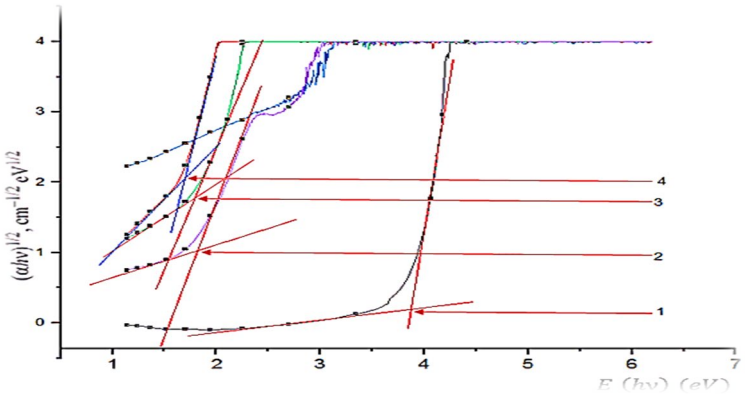

Fig. 9. Description of the light wavelength and energy (in eV) for photoanodes with different compositions, including FTO, FTO+glass, FTO+Glass+TiO_2, and FTO+Glass+TiO_2+Ru(x) with x ranging from 0.1 to 0.5.

At the next stage of photoanode preparation, with ruthenium-containing paint work was carried out to reduce the width of the forbidden zone, which leads to an increase in efficiency for photogeneration. In this case, the influence of ruthenium depending on the quantity and the time (in hours, days, and months) immersed in the paint was studied.

At the next stage of photoanode preparation, the photoconductivity characteristics of the electrode left for 126 days when using 0.2 percent of ruthenium paint were examined. The results of the experiment showed that there are differences between the samples left in the light and the dark place for a long time in the paint.

4. Conclusion

The purpose of studying the conductivity properties of the electrolyte was achieved. The dependence of conductivity on the amount of substances in the electrolyte was summarized as statistical data. The use of frequency dependence of the alternating current based on the impedance method was useful as a mathematical microscope for the studied object.

Results were obtained using I–V curve and impedance spectroscopy methods to study the conductivity of DSSCs prepared on the basis of five samples of 0.1-0.5mMn3. In this case, it was found that the photo galvanic quantities are useful for the 0.1 mMn3 sample when it is prepared using ultrasound.

When calculated based on the results obtained from the sample containing 0.2mMn3 ruthenium at room temperature, it was found that its useful work coefficient changed from 3.37 to 5.67 percent.

Descriptions obtained from the experimental results show that the mesoprosity property of TiO_2 was found to be the reason for the increased efficiency. The main reason for the increase in the number of absorbed photons was found to be an increase in the mesoprositic surface. It was not observed that the efficiency of FTO+TiO_2 photoanode and ITO+TiO_2 photoanode left in liquid paint for a long time did not change. If all experimental descriptions are viewed in one graph, it is possible to determine the factor of reducing the width of the prohibited zone to the working amount. When leaving the electrode in the paint for short periods of one or several tens of days, the time difference has a significant effect on the efficiency of the resulting semiconductor layer. However, in semiconductor layers prepared by leaving the paint for a long time, the length of the paint's ligeration time decreases. To see this in practice, all the descriptions were summarized in the same graphic description by summarizing the wavelengths or the energy values of the absorbed light.

In order to describe all the layers in the same graph, the steps of the wavelength of the light coming from the light source are performed using a computer in exactly the same steps in the case of an electronic device. Then, when combining the graphs, the wavelength on the X axis is set in nanometers (nm) or the energy in electron volts (eV) in appropriate values. This process would have taken a long time and with very poor resolution on equipment that was not automated and had software.

Availability of Data and Materials

The data and materials used in this study are available from the corresponding author upon reasonable request

Author Contributions

A.Q. Ergashov, S.B. Fazliddinov performed the experimental work; N.Yu. Sharibaev supervised the study; M.A. Yuldoshev served as the corresponding author; R.G. Ikramov reviewed and edited the manuscript; A.A. Abdulxayev drafted the manuscript.
All authors contributed to the critical revision of the manuscript for important intellectual content.
All authors read and approved of the final manuscript.
All authors have participated sufficiently in the work and agreed to be accountable for all aspects of the work.

Acknowledgements

We would like to express our sincere gratitude to everyone who supported us during the preparation of this manuscript. We also thank the peer reviewers for their valuable comments and constructive suggestions, which helped improve the quality of this work.

Funding

The research received no external funding.

Conflict of Interest

All authors certify that they have no conflicts of interest or professional relationships that might inappropriately affect the results presented in this research.

References

[1] R. Qohhar, E. Supriyanto, Sujito, A. T. Nugroho, A. Subekti, AIP Conference Proceedings **2278**(1), 020017 (2020). https://doi.org/10.1063/5.0015224
[2] S. Shalini, R. Balasundara Prabhu, S. Prasanna, T. K. Mallick, S. Senthilarasu, Renewable and Sustainable Energy Reviews **51**, 1306 (2015). https://doi.org/10.1016/j.rser.2015.07.052
[3] Y. Yang, et al., Advanced Materials **32**(7), 1904347 (2020). https://doi.org/10.1002/adma.201904347
[4] J. Wu, et al., Chemical Society Reviews **46**(19), 5975 (2017). https://doi.org/10.1039/C6CS00752J
[5] J. Wu, S. Wu, W. Sun, Electrochemistry Communications **122**, 106879 (2021). https://doi.org/10.1016/j.elecom.2020.106879
[6] J. Sun, et al., Electrochimica Acta **331**, 135282 (2020). https://doi.org/10.1016/j.electacta.2019.135282
[7] T. Akitsu, B. Miroslaw, S. Sudarsan, International Journal of Molecular Sciences **23**(17), 10005 (2022). https://doi.org/10.3390/ijms231710005
[8] A. Carella, F. Borbone, R. Centore, Frontiers in Chemistry **6**, 421 (2018). https://doi.org/10.3389/fchem.2018.00421

[9] M. Q. Lokman, et al., Micro & Nano Letters **16**(7), 395 (2021). https://doi.org/10.1049/mna2.12061
[10] V. F. Nunes, E. S. Teixeira, P. H. F. M. Júnior, A. F. L. Almeida, F. N. A. Freire, Cerâmica **68**(385), 75 (2022). https://doi.org/10.1590/0366-69132022683853219
[11] C. L. Ücker, et al., Chemical Physics Impact **4**, 100079 (2022). https://doi.org/10.1016/j.chphi.2022.100079
[12] Z.T. Azamatov, Sh.B. Utamuradova, M.A. Yuldoshev, N.N. Bazarbaev, East Eur. J. Phys. (2), 187 (2023). https://doi.org/10.26565/2312-4334-2023-2-19
[13] A. O. Oluwole, O. S. Olatunji, Environmental Sciences Europe **34**(1), 3 (2022). https://doi.org/10.1186/s12302-021-00588-7
[14] F. A. Giyasova, M. A. Yuldoshev, Chalcogenide Letters **22**(2), 123 (2025). https://doi.org/10.15251/CL.2025.222.123
[15] K. Sharma, V. Sharma, S. S. Sharma, Nanoscale Research Letters **13**, 381 (2018). https://doi.org/10.1186/s11671-018-2760-6
[16] J. Barichello, et al., Molecules **27**(13), 4178 (2022). https://doi.org/10.3390/molecules27134178
[17] G. Rossi, et al., International Journal of Photoenergy **2010**, 136807 (2010). https://doi.org/10.1155/2010/136807
[18] G. R. Li, J. Song, G. L. Pan, X. P. Gao, Energy & Environmental Science **4**(5), 1680 (2011). https://doi.org/10.1039/C1EE01105G
[19] L. Li, et al., Spectrochimica Acta Part A: Molecular and Biomolecular Spectroscopy **275**, 121192 (2022). https://doi.org/10.1016/j.saa.2022.121192
[20] T. G. Mayerhöfer, S. Pahlow, J. Popp, ChemPhysChem **21**(18), 2029 (2020). https://doi.org/10.1002/cphc.202000464
[21] S. R. Nishat, H. C. Chaudhari, A. H. Abdul Jaleel, Y. H. Shaikh, International Journal of Scientific & Technology Research **9**(3), 4858 (2020).
[22] G. Casasanta, F. Falcini, R. Garra, Journal of Photochemistry and Photobiology A: Chemistry **432**, 114086 (2022). https://doi.org/10.1016/j.jphotochem.2022.114086
[23] I. D. Anisimova, I. M. Vikulin, F. A. Zaitov, Sh. D. Kurmashev, Semiconductor Photodetectors, Radio i Svyaz, Moscow (1984).
[24] F.A. Giyasova, et al., East Eur. J. Phys. 4, 397 (2025). https://doi.org/10.26565/2312-4334-2025-4-38
[25] Sh.B. Utamuradova, F.A. Giyasova, K.N. Bakhronov, M.A. Yuldoshev, M.R. Bekchanova, B. Ismatov, East Eur. J. Phys. 3, 325 (2025). https://doi.org/10.26565/2312-4334-2025-3-31
[26] M.A. Yuldoshev, Z.T. Azamatov, A.B. Bakhromov, and M.R. Bekchanova, East Eur. J. Phys. (4), 250 (2024). https://doi.org/10.26565/2312-4334-2024-4-25
[27] Sh.B. Utamuradova, Z.T. Azamatov, A.I. Popov, M.R. Bekchanova, M.A. Yuldoshev, and A.B. Bakhromov, East Eur. J. Phys. (3), 278 (2024). https://doi.org/10.26565/2312-4334-2024-3-27
[28] M. M. Y. Missa, R. K. Pingak, H. I. Sutaji, Jurnal Fisika: Fisika Sains dan Aplikasinya **3**(1), 1 (2018). https://doi.org/10.35508/fisa.v3i1.606
[29] B. D. Viezbicke, S. Patel, B. E. Davis, D. P. Birnie, Physica Status Solidi (b) **252**(8), 1700 (2015). https://doi.org/10.1002/pssb.201552007
[30] J. B. Coulter, D. P. Birnie, Physica Status Solidi (b) **255**(3), 1700393 (2018). https://doi.org/10.1002/pssb.201700393
[31] L. L. G. Al-mahamad, Heliyon **8**(7), e09966 (2022). https://doi.org/10.1016/j.heliyon.2022.e09966
[32] Sh.B. Utamuradova, et al., Chalcogenide Letters, **22**(8), 753–764 (2025). https://doi.org/10.15251/CL.2025.228.753
[33] F.A. Giyasova, et al., East Eur. J. Phys. 4, 461 (2025). https://doi.org/10.26565/2312-4334-2025-4-47
[34] M. R. Mettu, A. Mallikarjun, M. Jaipal Reddy, J. Siva Kumar, Materials Today: Proceedings **62**(Part 2), 1045 (2022). https://doi.org/10.1016/j.matpr.2022.02.581
[35] O. S. Khukhlina, A. A. Antoniv, V. Y. Drozd, Ukrainian Therapeutic Journal **2019**(4), 20 (2019). https://doi.org/10.30978/UTJ2019-4-20
[36] S. T. Lee, D. H. Lee, S. K. Lim, Medžiagotyra **25**(3), 14246 (2019). https://doi.org/10.5755/j01.ms.25.3.14246